4D Flow when and how?

Yasuo Takehara[1]

Abstract

4D Flow is an emerging MR technique enabling three-dimensional and cardiac phase-resolved flowmetry with ECG-gated phase-contrast MRI that increased the speed of data acquisitions, accuracy and robustness. The method is promoting researches in areas that have not been fully addressed before in the cardiovascular system, such as flowmetry of the bloodstream across the valves, within the heart chambers, complexed flow dynamics such as vortex, helical or retrograde. Wall shear stress and other potential biomarkers derived from 4D Flow are known to be related to vascular wall diseases such as atherosclerosis. In this review, fundamental concepts of 4D Flow technique and post-processing, benefits and limitations as well as its clinical applications are discussed, and the importance of quality control and validation of the method is emphasized. New ideas inspired by 4D Flow can help clinicians and MR scientists further understand the role of flow dynamics in health sciences, diseases and various aspects of cardiovascular physiology.

Keywords Phase-contrast image · 4D Flow · Magnetic resonance · Flow analysis · Wall shear stress · Cardiovascular diseases

Introduction

Leonardo da Vinci, a universal genius who played an active part five hundred years ago in Italy, has been known to have an unusual interest in "flow." Since he was involved in civil engineering, such as irrigation, his obsession with the flow is easily understood. Since he was also an anatomist, his affinity to flow was naturally extended to blood flow. Among his anatomical illustrations of the heart, he has drawn a pair of vortex-like portions at the root of ascending aorta, the sinus of Valsalva [1], which was considered a "Da Vinci Code" for five hundred years (Fig. 1a). Today, we know that the vortices in the Valsalva sinus are created at diastole, which is hydrodynamically reasonable to the stable closure of the aortic valve (Fig. 1b, c). How could da Vinci reach a proper assumption? Could he depict the theoretical streamlines in his mind just based on the anatomical configurations? If so, he had a Navier–Stokes equation in his brain and executed a streamline analysis.

4D Flow technology

Nowadays, we can visualize the details of the flow dynamics within the human vessels in vivo with the use of innovative technique in MRI. Three-dimensional (3D) cine phase-contrast MRI (PC) or 4D Flow MRI (Fig. 1b–e) is a new MR technique that can measure the moving speed of hydrogen nuclei (protons) in a region of interest in 3D fashion and phase-resolved manner with ECG gating if you wish [2]. The essence of 4D Flow technology is the cine PC method. In addition to be able to visualize the blood flow, we can even quantify the complexity of the flow, not just velocity and flow rate (Fig. 1d, e).

MRI inherently has a function to measure proton velocity (Fig. 2) [3]. When gradient magnetic field is applied to an axis, for example, the x-axis direction, then the resonance frequency of the protons is linearly changed along the X-axis. After a specific duration of time, the phase shifts also occur linearly along the X-axis. Following this maneuver, another gradient magnetic field with the same strength but in the opposite direction is applied along the X-axis, and then,

✉ Yasuo Takehara
  takehara@med.nagoya-u.ac.jp

1   Department of Fundamental Development for Advanced
    Low Invasive Diagnostic Imaging, Nagoya University,
    Graduate School of Medicine, 65 Tsurumai-cho, Showa-ku,
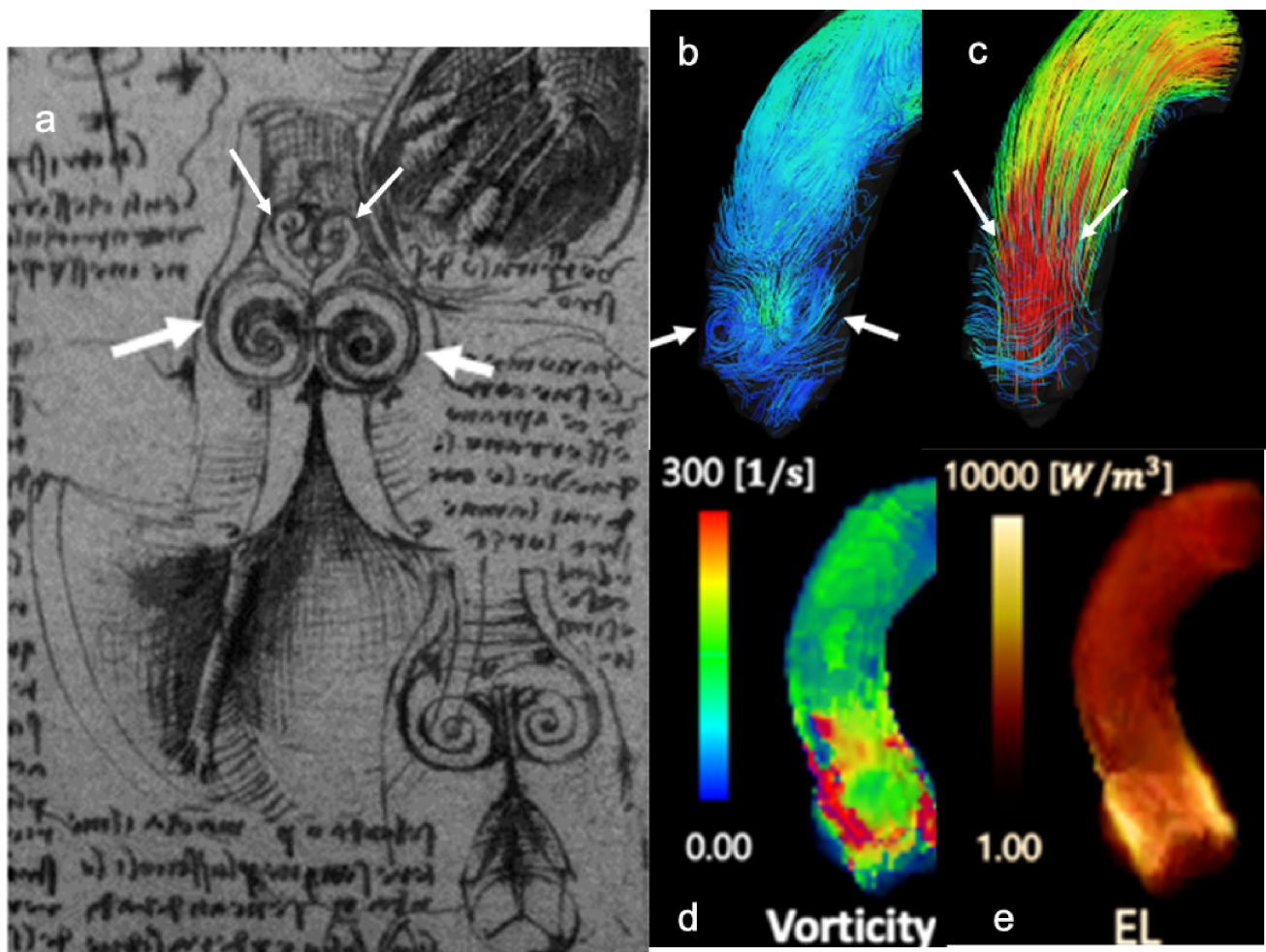   Nagoya, Aichi 466-8550, Japan

Fig. 1 a Leonard Da Vinci has drawn a pair of vortex-like portions at the root of ascending aorta (large arrows), the sinus of Valsalva. Today, we know that the vortices in the Valsalva sinus are created at diastole, which is hydrodynamically reasonable to the stable closure of the aortic valve. There are small vortices directly connected to the orifice of the aortic outflow (small arrows) probably reflecting outflow jets that appears in systole. **b** With streamline analysis using 4D Flow data, identical vortices are delineated at the corresponding portions at diastole and **c** outflow jets (small arrows) in systole. **d** A color-coded 3D vorticity map and **e** 3D energy loss map can be calculated and displayed

the same phenomenon occurs in the -X-axis direction. So the phase shifts created by the previous magnetic field gradient are canceled. For protons moving on the X-axis; however, the phase shift applied with the first magnetic field gradient cannot be canceled by the opposite gradient magnetic field, because they do not experience exactly the same local magnetic field and resultant phase shifts. If the individual phases of the protons vary within the same voxel, the signal of the imaging voxel will decrease. In this scheme of "degree of phase shift = reduced signal intensity = speed," the absolute value of the speed, therefore, can be measured by the signal intensity of the local voxels (Fig. 2). If this scheme is repeated for the three axes of X, Y and Z, with cardiac gating, it is possible to visualize the blood flow in four-dimensional fashion, i.e., spatial 3D + time (Fig. 3). This method is therefore called 4D Flow [2, 4]. To make it easy to understand

visually, signals on each X, Y, Z planes are translated into color-coded velocity vectors (Fig. 4a).

Velocity encoding and specific post-processing operations

For accurate velocity measurement with 4D Flow, it is vital to set velocity encoding (VENC) that matches the flow velocity of the region of interest. The strength of this gradient magnetic field is a measure for the flow velocity by replacing the phase difference between $-\pi$ and $+\pi$ with velocity. However, if the phase difference exceeds π, it is impossible to discriminate between α and $\pi + \alpha$. This phenomenon is called aliasing, which occurs when the set of VENC is too small. However, when VENC is too large, the
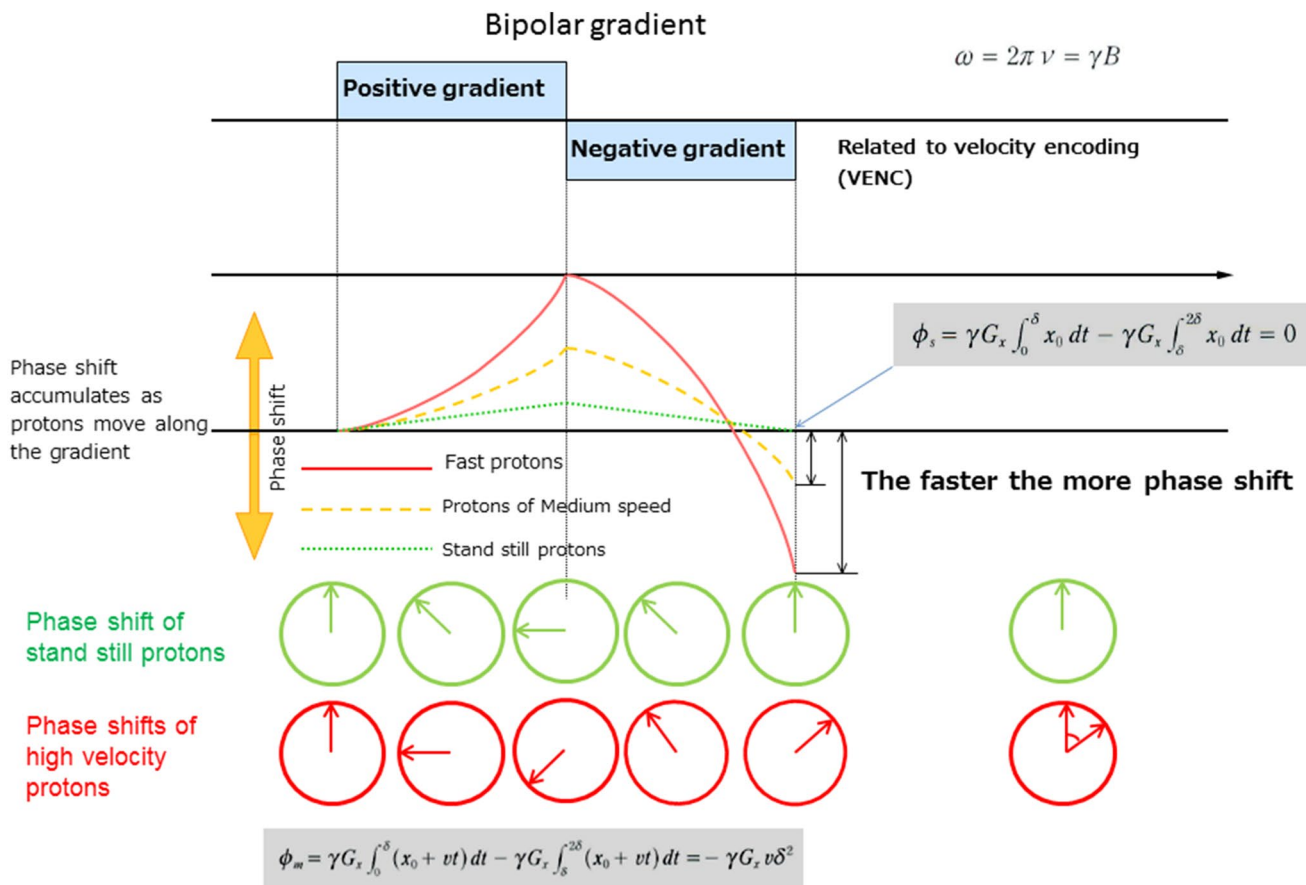
Bipolar gradient

$$\omega = 2\pi\,\nu = \gamma B$$

Positive gradient

Negative gradient

Related to velocity encoding (VENC)

Phase shift accumulates as protons move along the gradient

Phase shift

$$\phi_s = \gamma G_x \int_0^{\delta} x_0\, dt - \gamma G_x \int_{\delta}^{2\delta} x_0\, dt = 0$$

— Fast protons

--- Protons of Medium speed

······· Stand still protons

The faster the more phase shift

Phase shift of stand still protons

Phase shifts of high velocity protons

$$\phi_m = \gamma G_x \int_0^{\delta} (x_0 + vt)\, dt - \gamma G_x \int_{\delta}^{2\delta} (x_0 + vt)\, dt = -\gamma G_x v \delta^2$$

Fig. 2 To measure the velocity of the moving proton, a pair of gradient magnetic field (bipolar gradient) is applied along the *x*-axis. The proton standing still experiences phase shifts due to the additional positive gradient to original static magnetic field strength; however, the phase shift is canceled by the subsequent negative gradient of equal strength. When a proton is moving along the *x*-axis, it will experience additional static magnetic field strength, so the balance of phase shift becomes negative instead of zero. The vertical axis of the graph shows the amount of phase shift and the horizontal axis is time. Phase-contrast image replaces this augmented phase shift (= velocity) value with signal intensity

obtained phase difference is too small, which is responsible for a poor SNR, thereby resulting in poor velocity resolution. Since 4D Flow requires a relatively lengthy imaging time, repeated measurements with different VENC are not practical. Alternatively, in advance, the estimation of the maximum flow velocity of the measurement target has been done. Before imaging with 4D Flow, we perform a preliminary 2D PC with a large VENC and then minimize the VENC for 4D Flow. In this context, it is not reasonable to measure the arterial fast flow and venous slow flow together at the same time in one 4D Flow examination.

As the first step of post-processing, segmentation should be performed for fluid dynamic analysis (Fig. 4). In this process, overlaps of flow vectors of other vessels such as venous flows are excluded in the 3D model. The morphological information used for the segmentation is often MR angiography (MRA). After segmentation and interpolation with MRA, further assessments for the specific vessels are enabled (Figs. 4, 5). The segmentation should be done precisely using proper boundary information. If MRA used for the segmentation is misregistrated (spatially shifted), the post-processing data become inaccurate. Specifically, the flow velocity is calculated by the product of the cross-sectional area and the flow velocity. If the cross-sectional area is inaccurate or the actual vessel lumen vector is spatially shifted, it may be underestimated for low flow rate. Likewise, the wall shear stress (WSS) may be incorrectly higher or lower at the vessel boundary if the boundary information is inaccurate. It is because the wall shear stress (WSS) is a differential expression of the velocity gradient that changes as it approaches the wall.

There are many methods to characterize and visualize flow. Four standard methods, namely 3D vector field, 2D vector field, streamline and pathline or particle trace, are shown in Fig. 5a–d. Also, there are many derived indicators to assess flow such as WSS (Figs. 6a, b, 7a, d) or oscillatory shear index (OSI) (Fig. 7b). Nonlaminar or non-Womersley flow is decomposed into the helical flow and vortex flow.
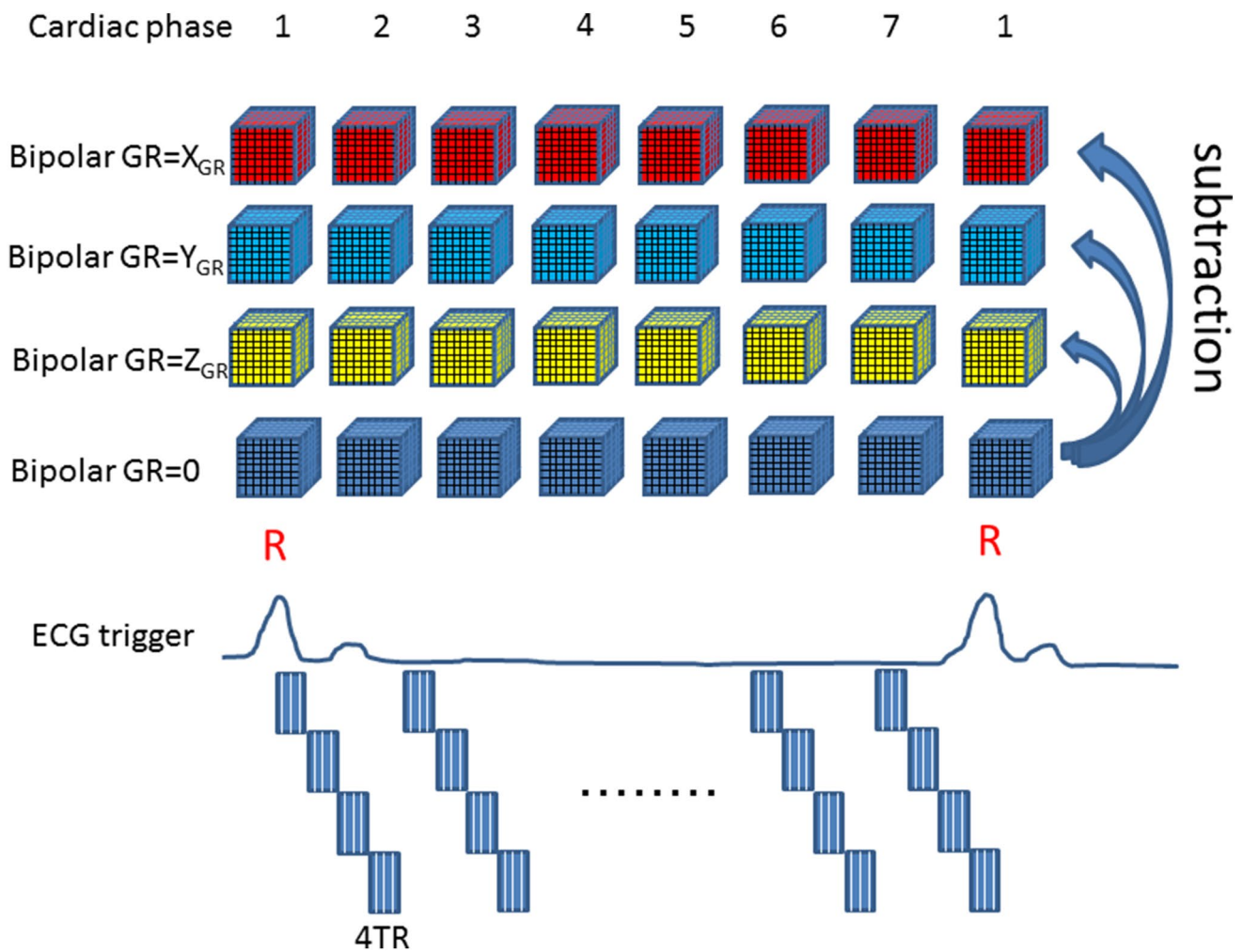
Fig. 3 To perform cardiac phase-resolved velocimetry in 3D fashion, it usually requires one hour or so with use of conventional phase-contrast images. Such data require reference and three flow-encoded excitations (Vx, Vy and Vz) for each phase-encoding view, spatial resolution, especially in the slice section-encoding direction, which makes its imaging time prohibitively lengthy. 4D Flow utilizes very efficient data sampling of heavy duty cycle, which had made this technique clinically viable. Phase-encoding scheme for an ECG-gated 4D Flow acquisition with flow encoding along all spatial directions and a selected slice encodes for each cardiac cycle (modified from Markl M, et al. JMRI 17:500, 2003)

Each has a scale of helicity and vorticity (Fig. 1d), and the degree can be measured. OSI is parameter of fluctuation for the WSS calculated by the formula shown in Fig. 7b.

Since the blood vessel is a three-dimensional structure, it is challenging to measure the WSS near the vessel wall in 2D fashion. With the advent of 4D Flow, practical analysis has been made possible, and thereby, its real significance is being understood in clinical practice. Abnormally low or high WSS and high OSI are known to be relevant biomarkers for pro-atherogenic factors (Fig. 8).

Essential benefits of 4D Flow

One of the unique advantages of 4D Flow is that en bloc flow velocity data can be acquired three-dimensionally with cardiac phase-resolved fashion, which means retrospective flowmetry is allowed for any vessels within the field of view. Unlike other modality like Doppler ultrasonography, the blood flow velocities of any vessels can be measured with arbitrary measurement sections even after patients left
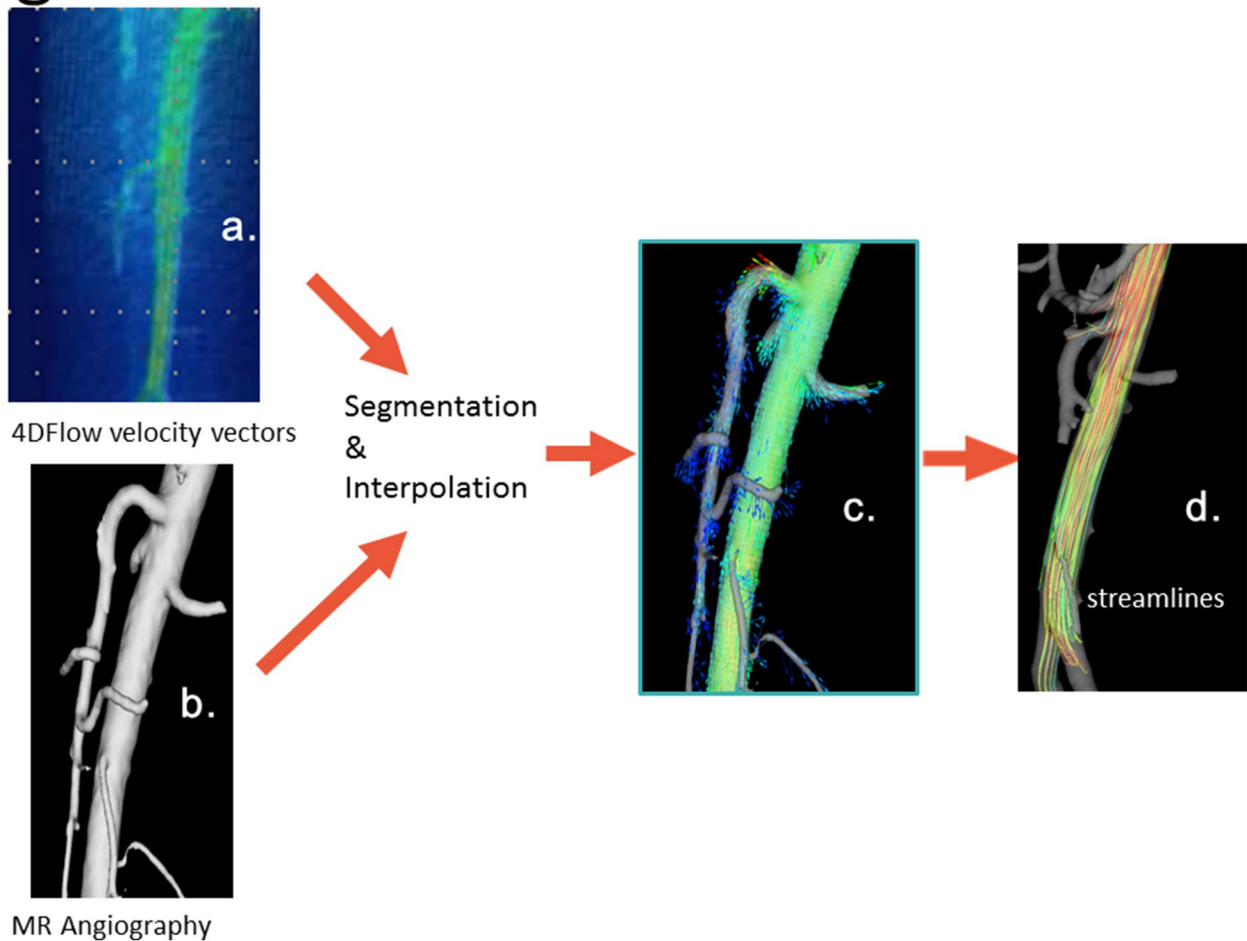
segmentation

Fig. 4 a 4D Flow allows whole three-dimensional velocity vector acquisition en bloc in cardiac phase-resolved fashion replacing velocity with signal intensity. Originally, all vectors are overlapped. **b** To assess only the artery, you should segment the velocity vectors from the original 3D data block. **b** MR angiography is used to segment the data focused on the vessels of interest. **c** Segmented velocity data are post-processed to **c** 3D vector field and then to the **d** streamlines

MR suite. This function is very convenient when multiple measurement points are required in one examination. The merit of this function is maximized in measuring the flow of each arterial branch of the transplanted kidney [5] or flow analysis for possibly responsible arteries for type II endoleak after endovascular repair (EVAR) for the abdominal aortic aneurysm [6, 7]. An attempt to measure the flow velocity and flow rate of certain blood vessels using the MR technique started 30 years ago, which had been an initial boom of MR flowmetry. For example, ischemia of the superior mesenteric artery (SMA) is a clinically interesting theme to be assessed by PC [8]. Dozens of researches have been performed using 2D cine PC since then [9–16]. Among these studies, some researchers noticed the fluctuations

in the measured flow velocity [17], but the discussion has not been sufficiently done on the reason why the fluctuations of the blood flow velocities occur. The flow velocity in the lumen is not necessarily laminar. Instead, there are many abnormal flows such as eddy, vortex and helical in the winded vessels or the pathological vessels. Taking one representative case, for example, Ishikawa et al. [18] had observed the improved flow in the renal artery after the percutaneous transluminal renal angioplasty (PTRA). The stenosed segment in the left renal artery was balloon-dilated for a patient suffering from renovascular hypertension, and then, her systemic blood pressure was normalized immediately. 4D Flow and CFD (computational fluid dynamics) were performed before and after the dilatation.
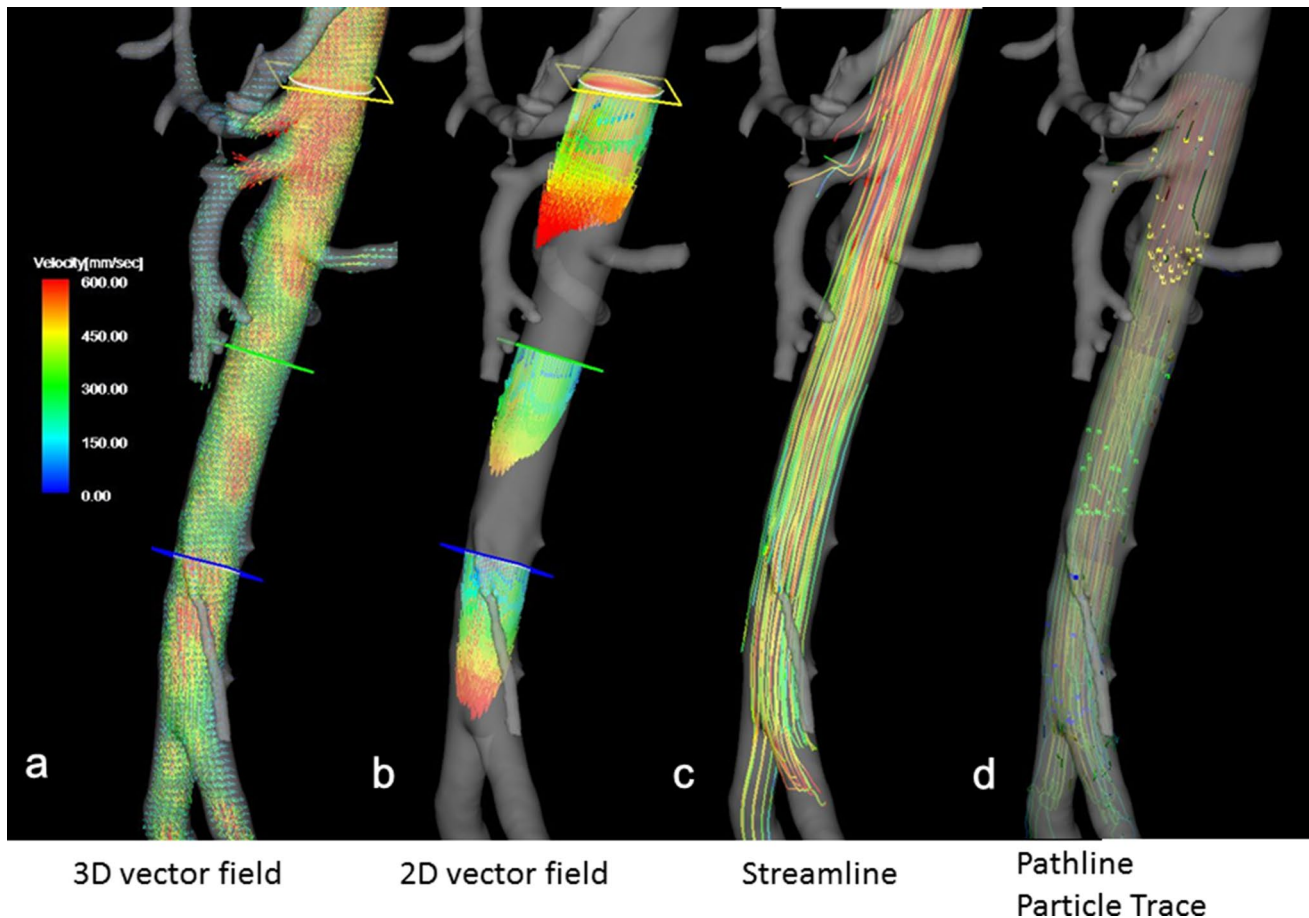
3D vector field | 2D vector field | Streamline | Pathline Particle Trace

Fig. 5 Since all the 4D (velocity in *x*, *y*, *z* + cardiac phase resolve) data are acquired en bloc, many types of visual post-processing are available. Flow visualization employed in fluid dynamics is used to make the flow patterns visible, to get qualitative or quantitative information on them. **a** 3D vector field is an assignment of a vector to each point in a subset of space. **b** A vector field in the plane (for instance), can be visualized as a collection of arrows with a given magnitude and direction, each attached to a point in the plane; 2D vector field). Vector fields are used to model the speed and direction of a moving fluid throughout space as it changes from one point to another point. **c** Streamline is lined connecting tandem velocity vectors. **d** Pathline or particle trace is a similar expression, but it connects velocity vectors moving to time (cardiac phases), which suggest the trajectory of the fluid movement

The time velocity patterns measured at the similar measurement planes before and after the intervention was different. Although the area under the curve increased after PTRA, the complexity of the streamlines in the flow path as well as the fluctuated time-velocity curve puzzled them. Before PTRA, vortex flow within the post-stenotic dilatation was dominant and fluctuation occurs in the measured values (Fig. 9b). With a close look at the streamline; however, it was easy to understand that the vortices in the post-dilated segment of the renal artery were responsible for this fluctuation. This phenomenon was also reproduced by the CFD simulations as well (Fig. 9). Also in flowmetry for healthy vessels, this problematic non-laminar flow should be kept in mind. Take superior mesenteric artery (SMA) for instance, physiological helical flow may be dominating at the curved portion (Fig. 10) [19]. Therefore, when we measure the flow velocity

and flow rate of specific vessels, we first perform streamline analysis with 4D Flow and then determine the measurement planes that can avoid abnormal flow. These flowmetry issues associated with complexed flow dynamics have not been fully discussed previously, probably because there has been no imaging technology to directly visualize the flow dynamics. Using these capabilities, 4D Flow is becoming an essential tool for qualitative and quantitative flowmetry for the vessels with complexed flow (Figs. 11, 12). For instance, Suwa et al. [20] found a fairly large whirlpool in the left atrium and the ventricle (Fig. 10) of the healthy volunteers, which was observed more often in individuals with normal cardiac function rather than degraded cardiac function [21].

From the viewpoint of blood delivery, vortex flow is not efficient. When a viscous liquid moves around randomly,

Fig. 6 One of the other advantages of 4D Flow is its ability to measure wall shear stress (WSS). **a** A scheme of the section of a vessel. The inner layer of the vessel is covered with endothelial cells. These cells have their mechanoreceptors of their own, which play the role of sensor for the WSS. Wall shear stress is, in a sense, like a frictional force like river stream eroding off the shore. Endothelial cells have the potential to monitor how fast the bloodstream is. **b** WSS can be defined as velocity vectors differential to normal coordinate perpendicular to the surface, which can be calculated by 4D Flow
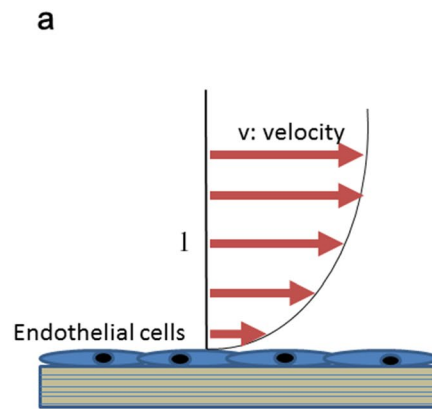
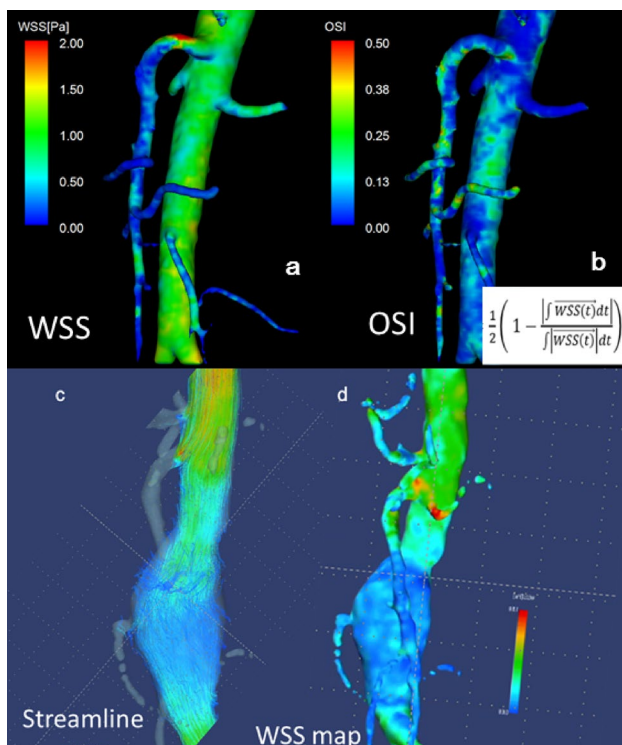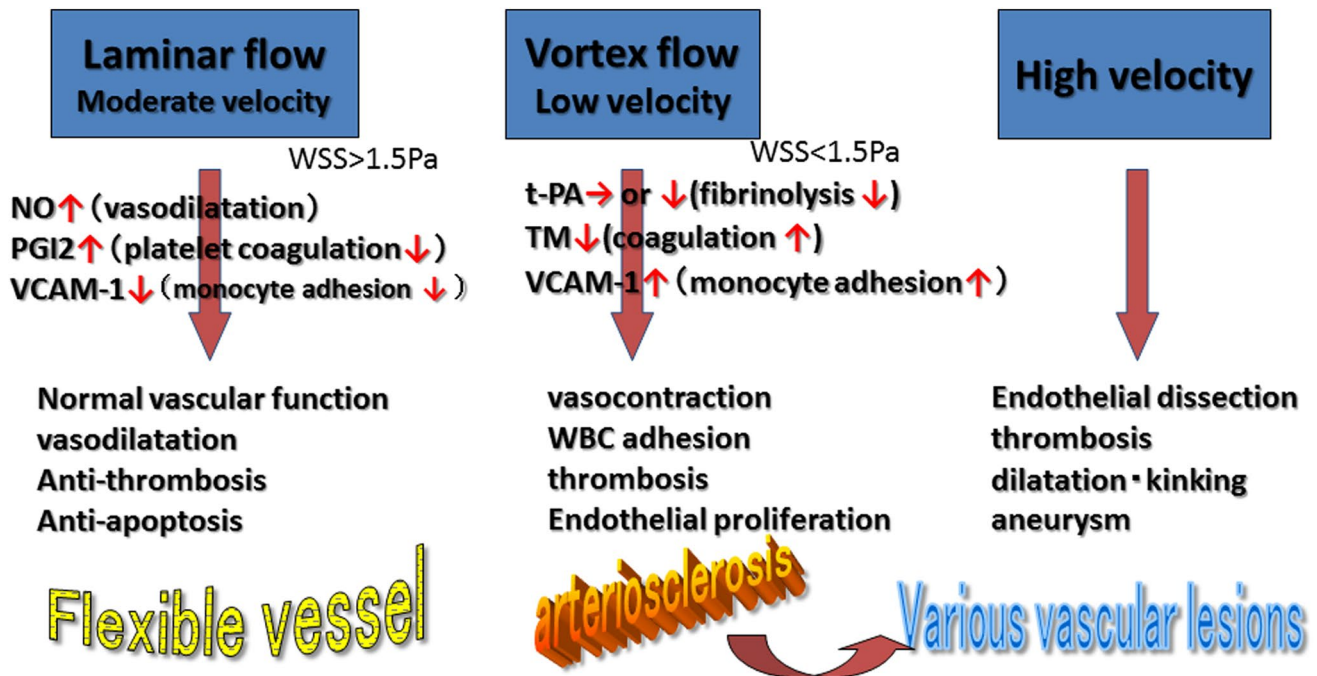$$(\text{shear stress}) = \mu \frac{dv}{dl}$$

μ: viscosity

Fig. 7 4D Flow provides entire 3D distributions of the flow vectors for each resolved time. **a** It is easy to create 3D wall shear stress (WSS) maps for each cardiac phase based on the acquired information. **b** Oscillatory shear index (OSI) is a parameter to show the fluctuation of the WSS. The more fluctuated, the more atherogenic signal the endothelial cells release. **c** Hemodynamic assessments of infrarenal abdominal aortic aneurysm (AAA) with streamline map and **d** Post-processed WSS map derived from the 4D Flow data. Note that the AAA wall is affected by low wall shear stress. Observing the streamline, it is noted that these low WSS was created by nonlaminar flow, i.e., turbulent or vortex flow

the kinetic energy is just converted into heat, resulting in an energy loss (Fig. 1e), which seems to be contributing nothing to blood circulation. However, it could also be assumed that the whirlpools in the heart may be helpful in maintaining the momentum of the flow during diastole, which may be analogous to the rational function of the vortices within the Valsalva sinus for aortic valve closure well depicted by da Vinci.

Vortices in the pulmonary trunk are related to pathological status. Terada et al. observed vortex flow in the pulmonary trunk of patients with pulmonary hypertension (Fig. 12). The complexed flow could be replaced by decreased WSSs and increased OSI of the pulmonary arteries, which were inversely correlated with pulmonary wedge pressures [22].

The validations and the quality control of 4D Flow

To propagate the appropriate use of 4D Flow technique in the clinical environment, it is necessary to properly validate the data by other standard measurement methods, such as Doppler ultrasonography (US), phantom experiments and CFD (computational fluid dynamics) (Figs. 9, 13). For the maximum velocity alone, Doppler US is reasonably correlated with 4D Flow velocimetry [5]. For the quality control of the MR system, there is a simple flow phantom analysis using a straight tube and a steady constant stream. According to Fukuyama et al., 4D Flow data acquisition should be

Laminar flow
Moderate velocity

WSS>1.5Pa

NO↑(vasodilatation)
PGI2↑(platelet coagulation↓)
VCAM-1↓(monocyte adhesion ↓)

Normal vascular function
vasodilatation
Anti-thrombosis
Anti-apoptosis

Flexible vessel

Vortex flow
Low velocity

WSS<1.5Pa

t-PA→ or ↓(fibrinolysis↓)
TM↓(coagulation↑)
VCAM-1↑(monocyte adhesion↑)

vasocontraction
WBC adhesion
thrombosis
Endothelial proliferation

arteriosclerosis

High velocity

Endothelial dissection
thrombosis
dilatation·kinking
aneurysm

Various vascular lesions

Modified from scheme of Malek et al. JAMA 282(21):2035-2042, 1999

Fig. 8 It is widely known that the laminar flow with moderate velocity is required to maintain the health of the artery. Arterial wall shear stress over 1.5 Pa is said to be required for atheroprotective effect, while vortex, turbulent or spiral flow with low velocity or low shear stress less than 0.4 Pa stimulates an atherogenic phenotypes and apoptosis of vascular smooth muscle cells, which promote atherosclerosis. Atherosclerosis ultimately leads arterial wall to various sorts of vascular diseases including aortic aneurysm or arteriosclerosis obliterans

performed with a spatial resolution of a certain level or more [23]. The error of the average flow velocity will be within 10% or less when a measured voxel is 30% or less than the cross-sectional area of the measured vessels. In the smaller tube of 3 mm in diameter, when the voxel size was 0.67 mm (22% of the straight pipe), the error of the cross-sectional average flow velocity increased up to 20%. This is because increased matrix size affected the SNR as a drawback (6). Well-balanced spatial resolution and the SNR are essential for accurate flowmetry in 4D Flow. A straightforward way to increase SNR is to employ higher magnetic field scanners and a phased array coil or contrast enhancement. Some researchers have started to use compressed sensing [24] and deep learning [25] to reduce noise effectively.

We also use in silico simulation, i.e., CFD for the validation of 4D Flow (Fig. 9), which is the theoretical simulation of flow dynamics using the Navier–Stokes equation. Since the preconditions are different, there are many cases where the results are slightly different. It should be a tool for cross-checking whether there are any significant inconsistencies. To date, the CFD analysis of cerebral aneurysms is reportedly similar to the findings by 4D Flow [26].

The limitations of 4D Flow

There are several limitations concerning the flowmetry with 4D Flow. One of the most serious ones is that 4D Flow can only depict the sum or average of hemodynamic events that repeat every cardiac cycle. This is a problem that is often encountered so long as data are collected with use of ECG gating. Therefore, it is challenging to reproduce other transient flows and fluctuations caused by respiration. For example, venous blood flow varies with the respiratory or other motions. One of the other technical limitations is that only one VENC can be set for one data acquisition. VENC may be rephrased as the magnitude of the bipolar gradient magnetic fieldset for each axis by the PC method. If the
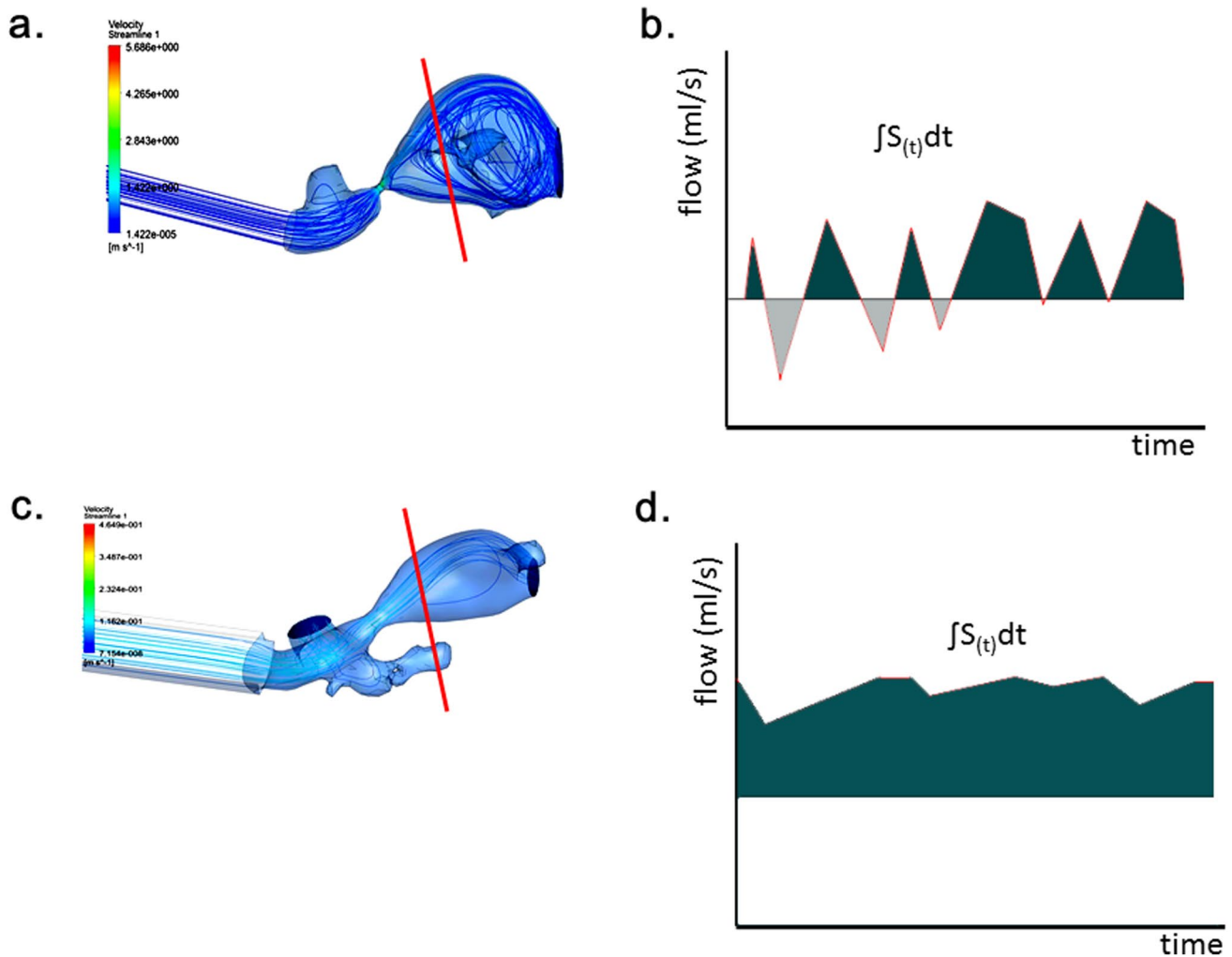
a.

b.

$\int S_{(t)} dt$

flow (ml/s)

time

c.

d.

$\int S_{(t)} dt$

flow (ml/s)

time

Fig. 9 CFD simulation for an individual of renovascular hypertension with left renal artery stenosis pre- and post-percutaneous transluminal renal angioplasty (PTRA). **a** Before PTRA, there is severe stenosis at the main left renal artery and subsequent post-stenotic dilatation. Note there are vortices in the post-stenotic dilatation. **b** The flow pattern becomes oscillatory in this type of vortex flow. **c** After PTRA, the vortex flow subsided. **d** The flowmetry at the same portion became less oscillatory. To measure this type of abnormal renal flow dynamics, the area under the curve should be measured after an appropriate temporal resolution

VENC setting is too low, aliasing will occur, and if it is too high, the SNR of the flow rate will deteriorate. This small degree of freedom is a problem because the accuracy of flowmetry is dependent on SNR. Concerning the issue of uniform VENC, dual VENC setting has appeared as a work-in-progress. However, brief imaging time for 4D Flow is a prerequisite for the dual VENC. For this purpose, sparse imaging such as compressed sensing and kt has already been applied, and in the future, it is desired to collect data with improved SNR and improved spatial resolution by using deep learning [27]. Further innovations in 4D Flow imaging technology are awaited.

Conclusion

The flow velocity measurement by 4D Flow and the derived indices were described. We do hope the correct use and evaluation of this new technology will satisfy clinical requirements.
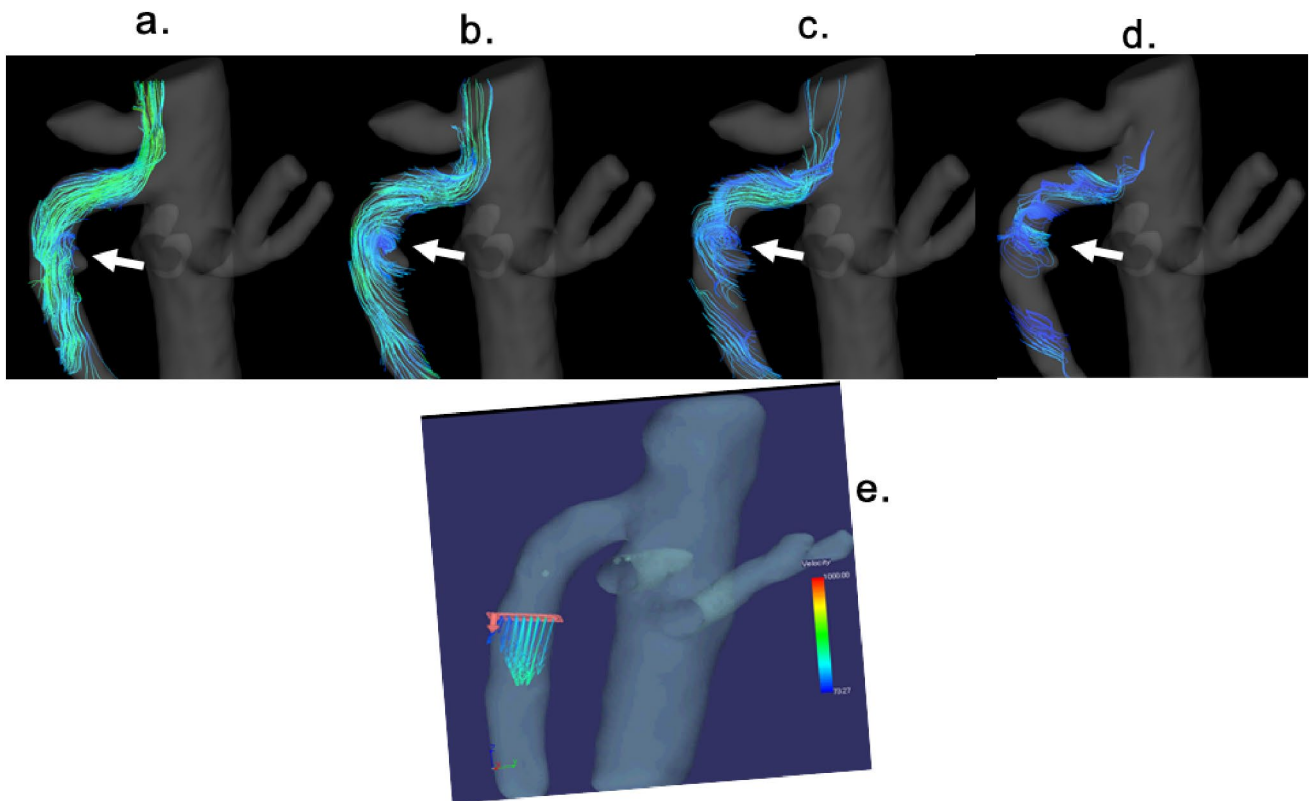
Fig. 10 Even in the healthy vessels, curved flow path creates non-laminar flow. The superior mesenteric artery, for example, **a–d** helical flow is dominant at the curved segment (arrow). **e** To measure the proper flow of this vessel, distal straight segment where the flow is laminar should be selected. Streamlines delineated helical flow at the curved segment of the SMA from **a** systole to **d** diastole. After depiction of the flow, appropriate flowmetry segment is selected, and the distal straight segment was chosen. **e** Note a parabolically lined flow vectors, which indicates normal laminar flow

Fig. 11 There is a physiological large vortex flow within the left atrium (arrow) seen in a healthy volunteer. The individuals with normal cardiac function usually maintain this type of vortex flow. Streamline analysis of the whole heart in **a** left anterior oblique view and **b** right anterior oblique view
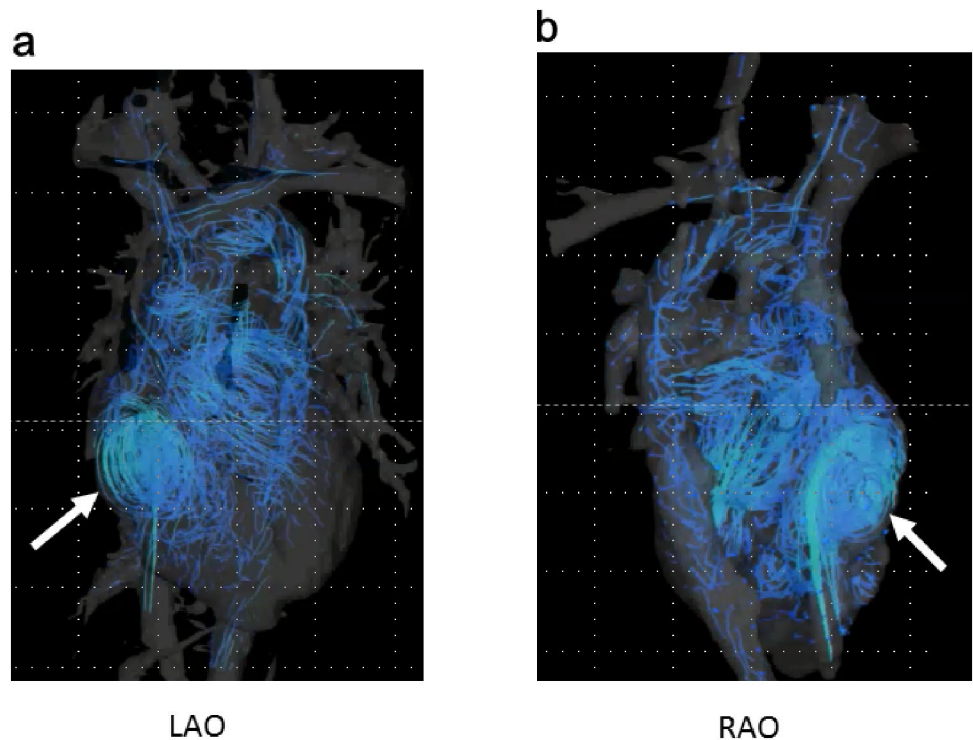
Fig. 12 Streamline analysis for the pulmonary artery at systole of **a** a normal and **b** a patient affected by pulmonary hypertension. There is mostly laminar flow in the normal pulmonary artery; however, in the pulmonary hypertension, a helical flow within the right pulmonary artery and the vortex flow in the main trunk of the pulmonary artery (arrows) are dominant
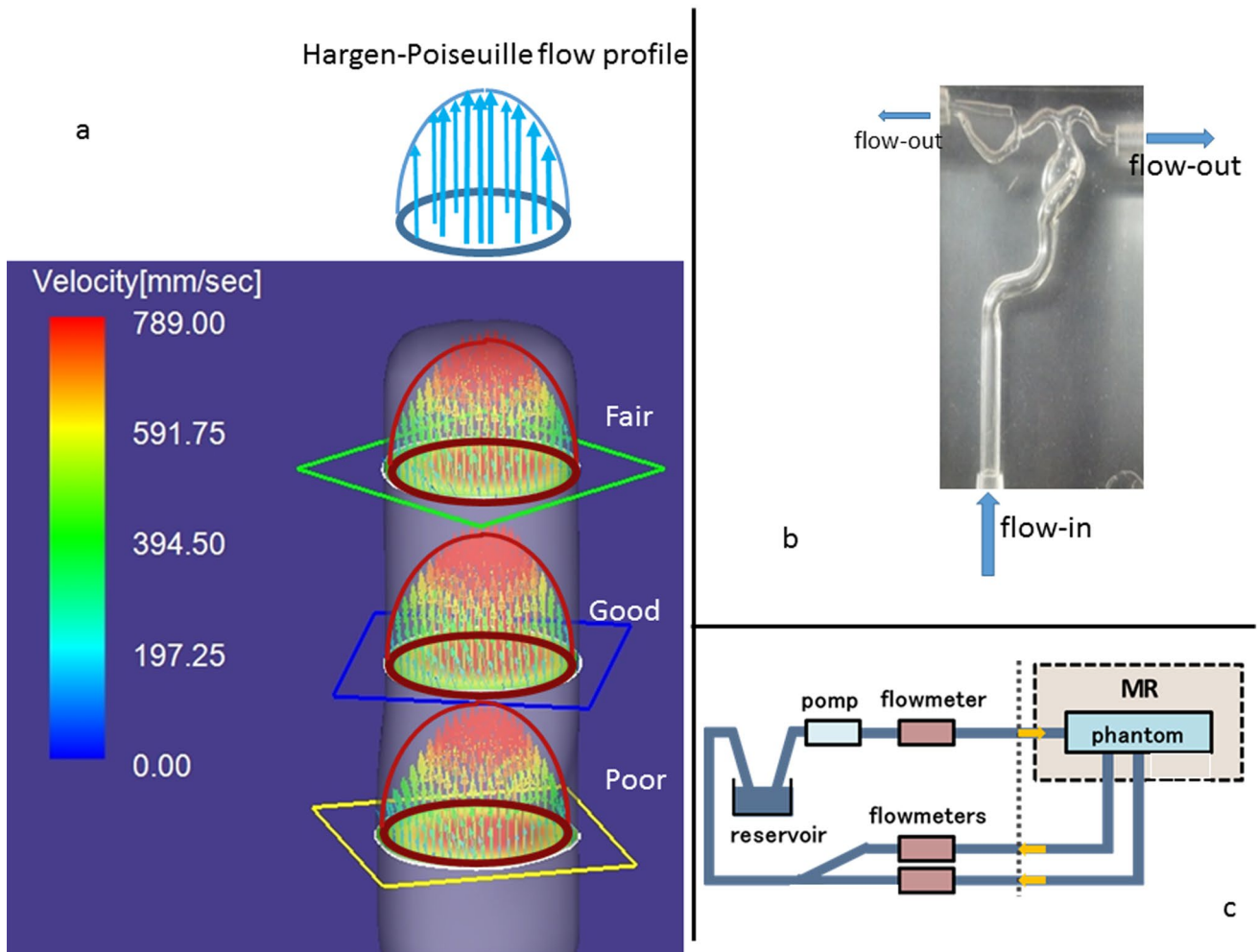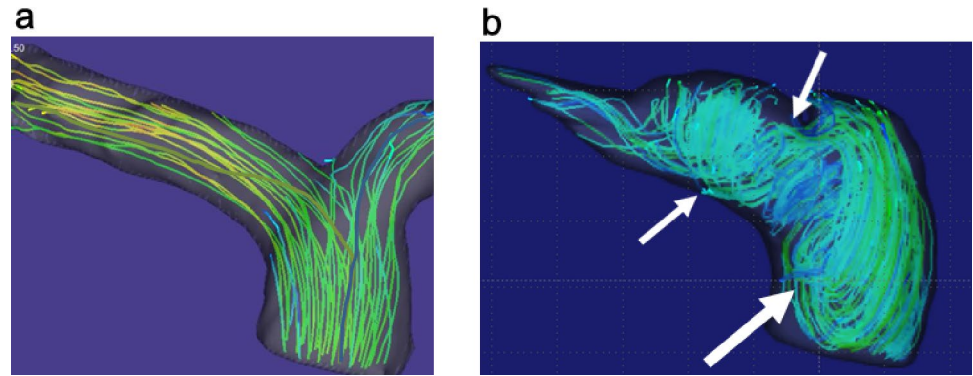

Fig. 13 a Flow profile validation using straight tube. Since 4D Flow provides 3D data, the flow profiles in the circular pipe can be analyzed in all directions of XYZ. This way, the profile of the flow velocity can be checked. The Womersley flow should be laminar and the profile is symmetrically parabolic. This assessment is particularly important in measuring proper wall shear stress. After assessing the straight pipe with steady constant flow, **b** 3D printed individual flow phantom model made of silicon can be assessed. **c** Computer-controlled pulsatile flow pump can be used for further assessments of more complexed flow dynamics

Compliance with ethical standards

References

1. Wells F (2013) The heart of Leonardo. Springer, Heidelberg
2. Markl M, Draney MT, Hope MD, Levin JM, Chan FP, Alley MT, Pelc NJ, Herfkens RJ (2004) Time-resolved 3-dimensional velocity mapping in the thoracic aorta: visualization of 3-directional blood flow patterns in healthy volunteers and patients. J Comput Assist Tomogr 28(4):459–468
3. Pelc LR, Pelc NJ, Rayhill SC, Castro LJ, Glover GH, Herfkens RJ, Miller DC, Jeffrey RB (1992) Arterial and venous blood flow: noninvasive quantitation with MR imaging. Radiology 185(3):809–812. https://doi.org/10.1148/radiology.185.3.1438767
4. Markl M, Pelc NJ (2004) On flow effects in balanced steady-state free precession imaging: pictorial description, parameter dependence, and clinical implications. J Magn Res Imaging JMRI 20(4):697–705. https://doi.org/10.1002/jmri.20163
5. Motoyama D, Ishii Y, Takehara Y, Sugiyama M, Yang W, Nasu H, Ushio T, Hirose Y, Ohishi N, Wakayama T, Kabasawa H, Johnson K, Wieben O, Sakahara H, Ozono S (2017) Four-dimensional phase-contrast vastly undersampled isotropic projection reconstruction (4D PC-VIPR) MR evaluation of the renal arteries in transplant recipients: preliminary results. J Magn Res Imaging JMRI 46(2):595–603. https://doi.org/10.1002/jmri.25607
6. Katahashi K, Sano M, Takehara Y, Inuzuka K, Sugiyama M, Alley MT, Takeuchi H, Unno N (2019) Flow dynamics of type II endoleaks can determine sac expansion after endovascular aneurysm repair using four-dimensional flow-sensitive magnetic resonance imaging analysis. J Vasc Surg 70(1):107e101–116e101. https://doi.org/10.1016/j.jvs.2018.09.048
7. Sakata M, Takehara Y, Katahashi K, Sano M, Inuzuka K, Yamamoto N, Sugiyama M, Sakahara H, Wakayama T, Alley MT, Konno H, Unno N (2016) Hemodynamic analysis of endoleaks after endovascular abdominal aortic aneurysm repair by using 4-dimensional flow-sensitive magnetic resonance imaging. Circ J 80(8):1715–1725. https://doi.org/10.1253/circj.CJ-16-0297
8. Naganawa S, Cooper TG, Jenner G, Potchen EJ, Ishigaki T (1994) Flow velocity and volume measurement of superior and inferior mesenteric artery with cine phase contrast magnetic resonance imaging. Radiat Med 12(5):213–220
9. Ayukawa Y, Murayama S, Tsuchiya N, Yara S, Fujita J (2011) Estimation of pulmonary vascular resistance in patients with pulmonary fibrosis by phase-contrast magnetic resonance imaging. Jpn J Radiol 29(8):563–569. https://doi.org/10.1007/s11604-011-0598-2
10. Barthelmes D, Parviainen I, Vainio P, Vanninen R, Takala J, Ikonen A, Tueller D, Jakob SM (2009) Assessment of splanchnic blood flow using magnetic resonance imaging. Eur J Gastroenterol Hepatol 21(6):693–700. https://doi.org/10.1097/MEG.0b013e32831a86e0
11. Dalman RL, Li KC, Moon WK, Chen I, Zarins CK (1996) Diminished postprandial hyperemia in patients with aortic and mesenteric arterial occlusive disease. Quantification by magnetic resonance flow imaging. Circulation 94(9 Suppl):II206–II210
12. Jeays AD, Lawford PV, Gillott R, Spencer P, Barber DC, Bardhan KD, Hose DR (2007) Characterisation of the haemodynamics of the superior mesenteric artery. J Biomech 40(9):1916–1926. https://doi.org/10.1016/j.jbiomech.2006.09.009
13. Machida H, Komori Y, Ueno E, Shen Y, Hirata M, Kojima S, Morita S, Sato M, Okazaki T (2009) Spatial factors for quantifying constant flow velocity in a small tube phantom: comparison of phase-contrast cine-magnetic resonance imaging and the intraluminal Doppler guidewire method. Jpn J Radiol 27(9):335–341. https://doi.org/10.1007/s11604-009-0349-9
14. Machida H, Komori Y, Ueno E, Shen Y, Hirata M, Kojima S, Sato M, Okazaki T, Masukawa A, Morita S, Suzuki K (2010) Accurate measurement of pulsatile flow velocity in a small tube phantom: comparison of phase-contrast cine magnetic resonance imaging and intraluminal Doppler guidewire. Jpn J Radiol 28(8):571–577. https://doi.org/10.1007/s11604-010-0472-7
15. Takahashi H, Tanaka H, Fujita N, Murase K, Tomiyama N (2011) Variation in supratentorial cerebrospinal fluid production rate in one day: measurement by nontriggered phase-contrast magnetic resonance imaging. Jpn J Radiol 29(2):110–115. https://doi.org/10.1007/s11604-010-0525-y
16. Tsuchiya N, Ayukawa Y, Murayama S (2013) Evaluation of hemodynamic changes by use of phase-contrast MRI for patients with interstitial pneumonia, with special focus on blood flow reduction after breath-holding and bronchopulmonary shunt flow. Jpn J Radiol 31(3):197–203. https://doi.org/10.1007/s11604-012-0171-7
17. Li KC, Whitney WS, McDonnell CH, Fredrickson JO, Pelc NJ, Dalman RL, Jeffrey RB Jr (1994) Chronic mesenteric ischemia: evaluation with phase-contrast cine MR imaging. Radiology 190(1):175–179. https://doi.org/10.1148/radiology.190.1.8259400
18. Ishikawa T, Takehara Y, Yamashita S, Iwashima S, Sugiyama M, Wakayama T, Johnson K, Wieben O, Sakahara H, Ogata T (2015) Hemodynamic assessment in a child with renovascular hypertension using time-resolved three-dimensional cine phase-contrast MRI. J Magn Res Imaging JMRI 41(1):165–168. https://doi.org/10.1002/jmri.24522
19. Sugiyama M, Takehara Y, Kawate M, Ooishi N, Terada M, Isoda H, Sakahara H, Naganawa S, Johnson KM, Wieben O, Wakayama T, Nozaki A, Kabasawa H (2020) Optimal plane selection for measuring post-prandial blood flow increase within the superior mesenteric artery: analysis using 4D flow and computational fluid dynamics. Magn Reson Med Sci. https://doi.org/10.2463/mrms.mp.2019-0089
20. Suwa K, Saitoh T, Takehara Y, Sano M, Nobuhara M, Saotome M, Urushida T, Katoh H, Satoh H, Sugiyama M, Wakayama T, Alley M, Sakahara H, Hayashi H (2015) Characteristics of intra-left atrial flow dynamics and factors affecting formation of the vortex flow—analysis with phase-resolved 3-dimensional cine phase contrast magnetic resonance imaging. Circ J 79(1):144–152. https://doi.org/10.1253/circj.CJ-14-0562

21. Suwa K, Saitoh T, Takehara Y, Sano M, Saotome M, Urushida T, Katoh H, Satoh H, Sugiyama M, Wakayama T, Alley M, Saka-hara H, Hayashi H (2016) Intra-left ventricular flow dynamics in patients with preserved and impaired left ventricular function: analysis with 3D cine phase contrast MRI (4D-Flow). J Magn Res Imaging JMRI 44(6):1493–1503. https://doi.org/10.1002/jmri.25315

22. Terada M, Takehara Y, Isoda H, Uto T, Matsunaga M, Alley M (2016) Low WSS and high OSI measured by 3D cine PC MRI reflect high pulmonary artery pressures in suspected second-ary pulmonary arterial hypertension. Magn Reson Med Sci 15(2):193–202. https://doi.org/10.2463/mrms.mp.2015-0038

23. Fukuyama A, Isoda H, Morita K, Mori M, Watanabe T, Ishiguro K, Komori Y, Kosugi T (2017) Influence of spatial resolution in three-dimensional cine phase contrast magnetic resonance imag-ing on the accuracy of hemodynamic analysis. Magn Reson Med Sci 16(4):311–316. https://doi.org/10.2463/mrms.mp.2016-0060

24. Ma LE, Markl M, Chow K, Huh H, Forman C, Vali A, Greiser A, Carr J, Schnell S, Barker AJ, Jin N (2019) Aortic 4D flow MRI in 2 minutes using compressed sensing, respiratory controlled adap-tive k-space reordering, and inline reconstruction. Magn Reson Med 81(6):3675–3690. https://doi.org/10.1002/mrm.27684

25. Retson TA, Besser AH, Sall S, Golden D, Hsiao A (2019) Machine learning and deep neural networks in thoracic and car-diovascular imaging. J Thorac Imaging 34(3):192–201. https://doi.org/10.1097/RTI.0000000000000385

26. Watanabe T, Isoda H, Takehara Y, Terada M, Naito T, Kosugi T, Onishi Y, Tanoi C, Izumi T (2018) Hemodynamic vascular biomarkers for initiation of paraclinoid internal carotid artery aneurysms using patient-specific computational fluid dynamic simulation based on magnetic resonance imaging. Neuroradiol-ogy 60(5):545–555. https://doi.org/10.1007/s00234-018-2002-8

27. Bratt A, Kim J, Pollie M, Beecy AN, Tehrani NH, Codella N, Perez-Johnston R, Palumbo MC, Alakbarli J, Colizza W, Drexler IR, Azevedo CF, Kim RJ, Devereux RB, Weinsaft JW (2019) Machine learning derived segmentation of phase velocity encoded cardiovascular magnetic resonance for fully automated aortic flow quantification. J Cardiovasc Magn Reson 21(1):1. https://doi.org/10.1186/s12968-018-0509-0

Publisher's Note Springer Nature remains neutral with regard to jurisdictional claims in published maps and institutional affiliations.